Meccanica (2007) 42:19–29
DOI 10.1007/s11012-006-9018-6

Determination of mechanical properties by instrumented indentation

Jaroslav Menčík

Received: 18 April 2006 / Accepted: 4 June 2006 / Published online: 21 October 2006

Abstract The paper reviews the current state of the depth-sensing indentation (sometimes called nanoindentation), where the information on material behaviour and properties is obtained from the indenter load and depth, measured continuously during loading and unloading. It is shown how the contact parameters and principal characteristics are determined using pointed or spherical indenters. Indentation tests can be used for the measurement of hardness and elastic modulus, and also of the yield stress and for the construction of stress–strain diagrams, for the determination of the work of indentation and its components. Most devices use monotonic loading and unloading, but some also enable measurement under a small harmonic signal added to the basic monotonously increasing load. This makes possible continuous measurement of contact stiffness and the study of dynamic properties and the determination of properties of coatings. One section is devoted to the measurement on viscoelastic-plastic materials, where the delayed deforming must be considered during the measurement as well as in data evaluation. Instrumented indentation can also be used for the study of creep under high temperatures. The paper also discusses the errors arising in depth-sensing measurements and informs briefly about some other possibilities of the method.

Keywords Mechanical properties · Measurement · Indentation · Hardness · Mechanics of solids

J. Menčík (✉)
Jan Perner Transport Faculty,
KPSDM, University of Pardubice,
Studentská 95, CZ-53210 Pardubice,
Czech Republic
e-mail: jaroslav.mencik@upce.cz

1 Introduction

Instrumented indentation, called also depth-sensing indentation, determines the contact parameters not from direct observation of the imprint, but from the indenter load and depth, measured continuously during loading and unloading (Fig. 1). This can yield much more information about material properties than the common hardness testing. The most important material characteristics from depth-sensing indentation are hardness and elastic modulus, but the method is also capable of determining the yield stress, strain hardening exponent, parameters of viscoelastic response or creep, and even some fracture mechanics parameters. The devices for instrumented indentation are usually equipped with a video microscope, which makes possible the observation of imprints and surrounding area.

Highly sensitive sensors, together with computer control enable measurement under loads as low as several mN, with corresponding depths of

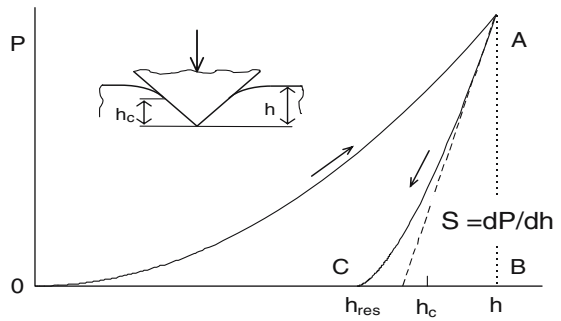

Fig. 1 Load–depth curves of an indentation test—a schematic

penetration tens or hundreds of nanometers. In this case, the method, referred to as *nanoindentation*, is especially suitable for the measurement of properties of thin surface layers, coatings and very small volumes. It is used mostly in the development or manufacture of new materials and special components mechanical, electrical or optical, but also in the research of biological tissues. The current nanoindenters are designed mostly for laboratory use. However, they can also be used for the determination of material properties of large structures. In such case, only very small specimen (several mm) must be cut off, so that the damage to the structure is very small. With the size of permanent imprints of the order of μm or less, the method itself is nearly nondestructive.

The depth-sensing indentation was developed originally for very low loads and small imprints. However, the method is quite general. Due to its advantages, today also some hardness testers for high loads are equipped with facilities enabling continuous measurement of the indenter load and displacement and their analysis. Instrumented indentation was also included into the international standards ISO [1], and there are many publications about it, among others a monograph by Fischer-Cripps [2]. The following paper thus only wants to explain briefly its main features and possibilities, with emphasis on the new trends in the development and use.

2 Determination of contact parameters

Depth-sensing indentation was originally developed for testing of elastic-plastic materials, such as metals or ceramics, under monotonic loading and unloading. In this case, the data are usually processed by the manner proposed by Oliver and Pharr [3]. The contact depth h_c (Fig. 1) is calculated from the indenter load P, total penetration h and contact stiffness $S = dP/dh$ measured at the beginning of unloading:

$$h_c = h - \varepsilon \frac{P}{S}, \tag{1}$$

where ε is a constant ($\varepsilon \approx 0.75$). The contact stiffness S is obtained from a regression function (usually of power-law type) fitted to the unloading curve. The contact area A is calculated from contact depth, $A = f(h_c)$, with the calibration function f corresponding to the pertinent indenter. Today, some devices enable also the determination of contact stiffness under small harmonic oscillations; see the section about continuous stiffness measurement. More about the current state of knowledge about the determination of contact parameters can be found in the recent review paper by Oliver and Pharr [4].

3 Indenters

Two kinds of indenters are used: pointed and spherical (Fig. 2). *Pointed indenters* (Fig. 2a) have the shape of a pyramid or a cone. They cause high stress concentration at the tip, leading usually to plastic deformations or other irreversible processes in the tested material from the beginning of loading. The strain pattern depends on the tip angle, but it does not depend on the depth of penetration; the stress fields are self-similar and the contact pressure does not change with depth. This is especially advantageous when the depth-distribution of properties is to be studied.

The most often used pointed indenters are Berkovich and Vickers. Berkovich indenter, very common in nanoindentation, is a three-sided pyramid (more suitable for obtaining a sharper tip), with similar effective tip angle as the four-sided Vickers pyramid. In both cases, the tip angle of the equivalent cone (of the same volume) is 140.6°.

With *spherical indenters* (Fig. 2b), the ratio of contact depth to contact radius increases with the depth of penetration, and the characteristic strain under spherical indenter increases with relative

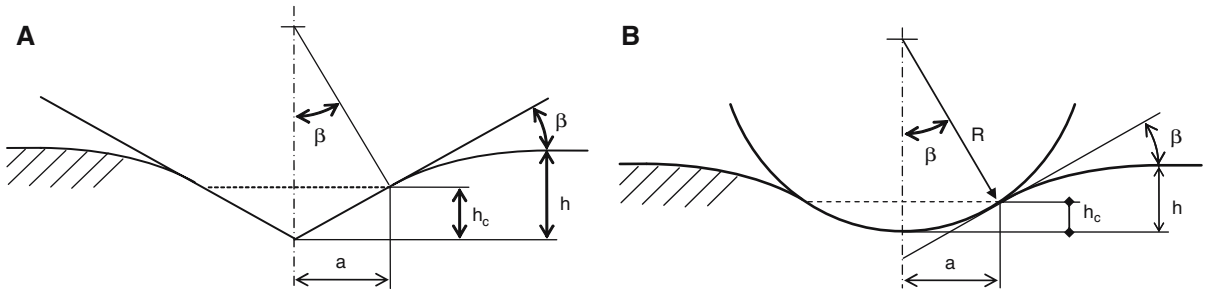

Fig. 2 Contact geometry: A—pointed indenter, B—spherical indenter

depth. This makes possible the characterisation of strain-dependent properties, such as strain hardening of metals. The deformations under spherical indenter are elastic first, and only from certain load they become elastic-plastic. The tip radius (decisive for the transition from elastic to elastic- plastic deforming), is usually of the order of 1–$10^2\mu$m for nanoindentation, and up to several mm for the tests in macro-scale or for investigation of elastic properties.

The indenters are usually made of diamond, but for testing of softer materials they can also be made from tungsten carbide or hardened steel. In an ideal case, the indenter shape can be described by a simple mathematical function (cone or sphere). Usually, however, the actual shape is more complex, e.g. due to difficulties in grinding and polishing, and calibration is necessary.

4 Hardness

In depth-sensing indentation, hardness H is defined as the mean contact pressure p_{m} under the loaded indenter, and is calculated as the indenter load P divided by the projected contact area A:

$$H = \frac{P}{A} = p_{\mathrm{m}}. \tag{2}$$

This definition can also be used for the analysis of contact stresses, and it is the only possible for highly elastic or hyper-elastic materials, such as rubber or diamond-like-carbon (DLC), where the imprint totally vanishes after unloading. Hardness is also measured in viscoelastic materials. Here, however, one must be aware that the contact depth (and H) depend not only on the load, but also on the duration of loading (see a special paragraph below).

5 Elastic modulus

From the indentation data, first the composite modulus E^* is determined from the contact stiffness S and contact area A:

$$E^* = \frac{\sqrt{\pi}}{2\beta}\,\frac{S}{\sqrt{A}}; \tag{3}$$

β is the correction factor for the indenter shape ($\beta \approx 1.07$; see Oliver and Pharr [4]). The Young modulus of the specimen, E, is then calculated from the composite modulus using the formula

$$\frac{1}{E^*} = \frac{1-\nu^2}{E} + \frac{1-\nu_i^2}{E_i}, \tag{4}$$

which reflects the fact that the total elastic compliance at the contact consists of the compliance of the specimen (no subscript) and the indenter (subscript i); ν means Poisson's ratio. The formula (3) is based on Sneddon's analysis [5] of penetration of various indenters into elastic half-space.

6 Yield strength and stress–strain diagrams

Yield stress Y can, in principle, be calculated from the mean contact pressure p_{m} (or hardness H) determined according to Eq. (2). It is also possible to construct "stress–strain" diagrams, similar to those from tensile tests. However, the situation is more complex, and until now, the results are often not satisfactory.

For soft metals with low hardness compared to elastic modulus, yield stress is usually calculated according to Tabor [6] as $Y = H/3$. For harder materials, this relationship does not hold, as the elastic deformations under the indenter are not negligible compared to the plastic ones. There are

also other aspects of indentation, which must be considered, if the results should be comparable with the data from simple tension or compression: the stress field in the contact area is inhomogeneous, the plastic deformations are localised, and the yield stress often depends on the degree of plastic deformation.

As a first step, a characteristic, or representative stress and strain in indentation tests must be defined. The representative stress is usually derived from the mean contact pressure as

$$\sigma_{\mathrm{rep}} = \frac{p_{\mathrm{m}}}{C}, \tag{5}$$

where C is so-called constraint factor. This factor is usually assigned the value 3, as found by Tabor and other researchers from the comparison of tensile and indentation tests on ductile metals. This fixed value, however, has some drawbacks, as will be shown later. The definition of representative strain depends on the indenter type. For pointed indenters, Tabor [6] proposed

$$\varepsilon_{\mathrm{rep}} = 0.2 \tan \beta, \tag{6}$$

where β is the angle between the indenter surface and the specimen (Fig. 2a). For Berkovich or Vickers indenter, $\beta = 19.7°$, so that the yield stress (5) corresponds not to the onset of plastic flow, but to a relatively large representative strain, about 7%. For another strain, an indenter with different tip angle must be used.

For stress–strain diagrams, spherical indenters are thus much more suitable. In this case, the representative strain can be defined (similarly to pointed indenters) by means of the angle between the specimen surface and the tangent to the indenter meridian at the edge of contact (Fig. 2b). As the angle β is usually small, $\tan \beta$ can be replaced by $\sin\beta$, which gives the common formula:

$$\varepsilon_{\mathrm{rep}} = 0.2 \ \frac{a}{R}, \tag{7}$$

where a is the contact radius and R is the radius of the indenter tip. However, the diagrams constructed for these σ_{rep} and $\varepsilon_{\mathrm{rep}}$ often differ from those for uniaxial loading, cf. Herbert et al. [7].

With spherical indenter, the deformations are elastic first, and the Hertzian formulae can be used; see Johnson [8]. The plastic flow occurs first for $p_{\mathrm{m}} = 1.1Y$. However, the volume of the plastically deformed material is negligible at the beginning, the curve P–h coincides with that for elastic loading, and only slowly it starts deflecting towards larger deformations, as the plasticised volume grows with increasing $\varepsilon_{\mathrm{rep}}$. At this stage, both elastic and plastic properties play a role. For $1.1Y < p_{\mathrm{m}} < 3Y$, Johnson [8] proposed the following relationship between hardness and yield strength (Fig. 3):

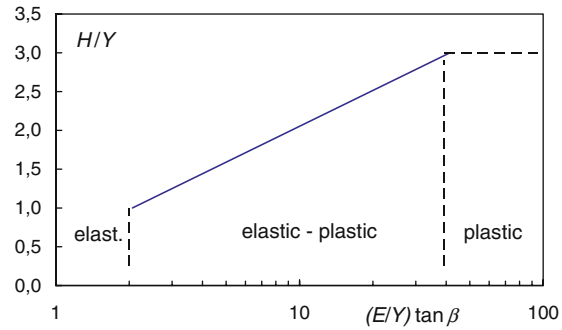

Fig. 3 Hardness to yield stress ratio as a function of material and contact parameters (after [8])

$$\frac{H}{Y} = \frac{2}{3}\left[2 + \ln\left(\frac{1}{3}\,\frac{E}{Y}\tan\beta\right)\right]. \tag{8}$$

For higher loads and strains, the plastic flow field is fully developed, and the ratio H/Y remains constant ($\approx$3).

Equation (8) can be transformed into a more general form:

$$\frac{p_{\mathrm{m}}}{Y} = A + B \ln\left(k\,\frac{E}{Y}\,\varepsilon_{\mathrm{rep}}\right), \tag{9}$$

where A, B and k are constants ($A \approx 4/3$, $B \approx 2/3$, $k \approx 5/3$). Actually, the right-hand part of Eq. (9) corresponds to the constraint factor C, which depends on $\varepsilon_{\mathrm{rep}}$ and the ratio E/Y that characterises the material susceptibility to plastic flow.

Thus, for $1.1 < p_{\mathrm{m}}/Y < 3$, the yield stress can be obtained from p_{m}, E and $\varepsilon_{\mathrm{rep}}$ by numerical solution of Eq. (9). For higher values of p_{m}/Y, the approximate formula $Y = p_{\mathrm{m}}/3$ should be used. In both cases, fitting the p_{m} values in a wider interval of $\varepsilon_{\mathrm{rep}}$ can be recommended.

The yield stress $Y(\varepsilon_{\mathrm{rep}})$, obtained in this way, should, in principle, correspond to the stress in the elastic-plastic part of the σ–ε diagram for simple compression. However, some differences can be expected. For example, extensive finite element analysis done by Mesarovic and Fleck [9] has shown that the relationship $p_{\mathrm{m}}(\varepsilon_{\mathrm{rep}})$ is linear not only to

the onset of plastic flow at $p_m = 1.1Y$, but as long as $p_m < 1.6Y$.

Also, the ratio $\sigma_{rep}/\varepsilon_{rep}$, calculated for elastic loading using the definitions (5), (7) and common values of C, is not equal E, in contrast to the ratio σ/ε in uniaxial loading. Thus, a more general analysis of this problem will be necessary for making both diagrams fully comparable. A work on this topic, with an improved procedure for the construction of stress–strain diagrams, was recently published by Menčík [10].

A somewhat different approach was proposed by Field and Swain [11]. The depth-sensing device UMIS makes possible the determination of the yield stress Y and the strain-hardening index not by numerical solution of the above equations, but by modelling the indentation response for the chosen material parameters, and comparing the simulated P–h curve with the experimental curve. In this way, their probable values can be found in several steps.

The strain-hardening index is a very useful characteristic for common metals. However, new materials with special properties, such as shape-memory alloys [12], have often complex course of $\sigma(\varepsilon)$, and stress–strain diagrams for a wide interval of strains are necessary.

7 Work of indentation

The loading and unloading curves P–h in depth-sensing tests can also yield information about energies involved in the process, such as the total work of indentation W_{tot} (area under the curve 0ABC0 in Fig. 1), the elastic work W_{el}, released during unloading (area CABC), and the plastic or irrecoverable energy W_{pl} (area 0AC0), which characterises the energy dissipated during the indentation plus the energy of residual stresses around the imprint. The energy components can be used for characterising plastic properties of the material. As the work depends on the indenter load, it is better to use normalised quantities, such as the *plasticity index* or *elasticity index*,

$$\omega_{pl} = \frac{W_{pl}}{W_{tot}}; \quad \omega_{el} = \frac{W_{el}}{W_{tot}} = 1 - \omega_{pl}. \tag{10}$$

For a homogeneous material and pointed indenter, the loading–unloading curves for different nominal loads are self-similar, so that the plasticity or elasticity index do not depend on load, and can be used as material characteristics.

It is also possible to analyse only parts of the P–h diagrams, and measure, for example, the work spent in some processes, such as formation and propagation of cracks or delamination, and use it for the determination of specific fracture energies.

For more details about energies in indentation processes, the reader is referred to Sakai [13] or Menčík and Swain [14].

8 Continuous stiffness measurement mode

Most depth-sensing indentation devices use monotonic loading and unloading, and the value of contact stiffness S is obtained from the unloading curve. Some devices also enable continuous stiffness measurement (so-called CSM mode), where a small harmonic signal (amplitude several nm or a fraction of a mN) is added to the monotonously increasing basic load. In this mode, the harmonic contact stiffness S_f is measured, defined as the ratio of the load and depth amplitudes of the small harmonic oscillations,

$$S_f = \frac{\Delta P}{\Delta h}; \tag{11}$$

the subscript f denotes the exciting frequency. In addition to S_f, also the shift between the load and displacement amplitudes (phase angle ψ) is measured.

The harmonic contact stiffness is measured continuously (Fig. 4), and makes possible the determination of properties during loading from "zero" to the maximum force (or from the surface to the maximum depth). In addition to S_f, also the "monotonic" contact stiffness $S = dP/dh$ is measured at the beginning of monotonic unloading from maximum load.

The CSM mode is especially suitable for materials with time-dependent response, such as plastics or biomaterials. For example, the harmonic elastic modulus, defined as

$$E_f^* = \frac{\sqrt{\pi}}{2\beta} \frac{S_f}{\sqrt{A}}, \tag{12}$$

can be used in design of components for dynamic loading. The phase angle informs about losses

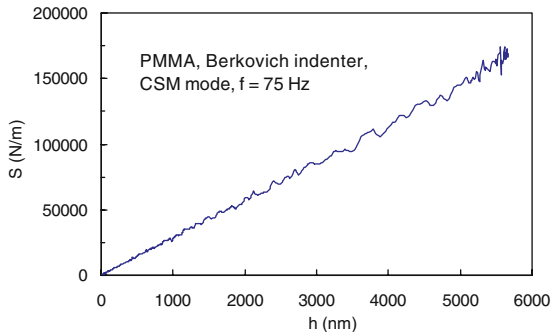

Fig. 4 Contact stiffness S as a function of indenter penetration h under harmonic loading (CSM mode)

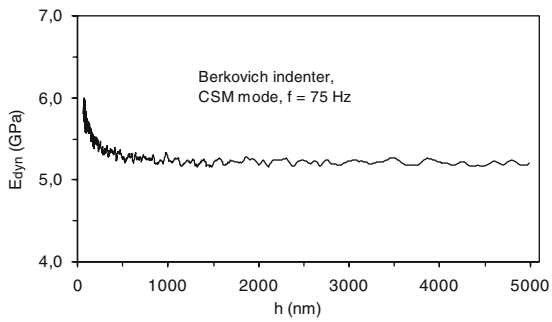

Fig. 5 Depth distribution of elastic modulus measured in CSM mode

caused by the internal friction in the material. The measurements can be done for various frequencies of oscillations (from several Hz to several hundred Hz), so that it is possible to study the dependence of the internal resistance on frequency. (See also the section on viscoelastic materials.)

Another useful application of the CSM mode is for specimens whose properties change with depth. Here, the property distribution can be obtained in a single test (Fig. 5), which makes the measurement much faster. This also holds for coated specimens, discussed below.

9 Determination of properties of coatings

Nanoindentation using very low loads (of the order of mN) is a very suitable means for the determination of mechanical properties of coatings or treated surfaces. However, the response during indentation is influenced by the properties of both the coating and substrate. The apparent (measured) value of some property $(E, H, \ldots)$ changes from that corresponding to the coating alone (for negligible penetration depth), to the substrate value for the penetration depth much larger than the coating or film thickness. Thus, the depth of penetration should be much smaller than the coating thickness, especially when the coating is harder or stiffer than the substrate. This is a difficult task, particularly for thin coatings (1 μm or less). Especially the apparent elastic modulus is influenced from the beginning of the indentation, more for larger difference between the elastic modulus of the coating and substrate. Therefore, the response is usually measured for various depths, and the genuine coating property is obtained by extrapolating the measured values to zero depth. The devices working in the CSM mode can yield the necessary $E(h)$ or $H(h)$ data in one test.

The apparent value of the pertinent property "X" (hardness, E-modulus, etc.), measured for the indenter penetration into depth h, can be expressed generally as

$$X(h) = X_{\mathrm{f}} w_{\mathrm{f}}(h) \quad + \quad X_{\mathrm{s}} w_{\mathrm{s}}(h), \tag{13}$$

where X_{f} and X_{s} is the value corresponding to the coating (film) and substrate, respectively, and w_{f} and w_{s} are weight factors, characterising the influence of the film and substrate on the indenter response at depth h. Another, only formally different expression is

$$X(h) = X_{\mathrm{f}} \Phi(h) \quad + \quad X_{\mathrm{s}}[(1 - \Phi(h)], \tag{14}$$

where

$$\Phi(h) = \frac{X(h) \quad - \quad X_{\mathrm{s}}}{X_{\mathrm{f}} \quad - \quad X_{\mathrm{s}}}, \tag{15}$$

is a dimensionless weight function, which decreases from 1 for $h = 0$ to zero for $h \gg t$, where t is the film thickness. It can be recommended to use in these formulae—instead of depth h—the relative depth of penetration x, expressed, for example, as $x = h/t$ or t/a, where a is the contact radius.

Various weight functions have been proposed. For *elastic modulus*, Menčík et al. [15] have compared and tested several functions, and recommended the expression based on the theoretical analysis of a layered elastic medium done by Gao et al. [16]. When processing the data using the above expressions, one should not forget that the

depth-sensing devices usually give the composite modulus E^* instead of E.

In the determination of *coating hardness*, two cases with principally different response can be distinguished: soft coating on a hard substrate, and a hard coating on a ductile substrate. While the plastic deformations are limited to the soft coating in the former case, a hard coating on a soft substrate deforms elastically and plunges into a relatively larger volume of plastically deformed substrate, and, eventually, breaks. There are many papers about the topic. Here, only two of them will be mentioned, based on physical models. Burnett and Rickerby [17] proposed the weight functions for hardness as the ratio of influenced volumes in the coating and substrate, while Jönsson and Hogmark [18] used the "area-law of mixtures", based on the ratio of contact areas. Some other approximations can be found in Bhattacharya and Nix [19] and Menčík [20].

10 Viscoelastic-plastic materials

The deformation of a viscoelastic–plastic material depends not only on the load magnitude, but also on its duration and time course. The indenter continues penetrating into the specimen also under constant load (Fig. 6), and sometimes even during the unloading.

The most appropriate characterisation of these materials is by means of rheological models, consisting of springs and dashpots, such as Maxwell body, Kelvin body, Standard Linear Solid, or their combinations, cf. Haddad [22] or Tschoegl [23].

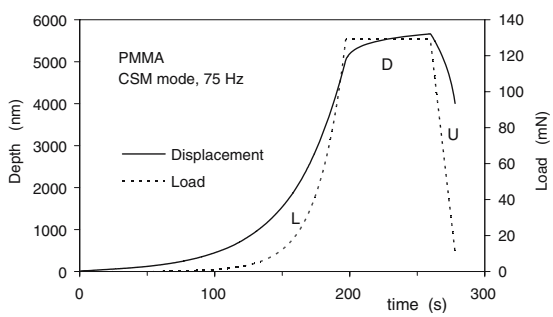

Fig. 6 Time course of a nanoindentation test into polymethylmethacrylate (PMMA) by Berkovich indenter [21]. L—loading, D—dwell, U—unloading

There are also papers on the determination of the pertinent constants by instrumented indentation, for example Strojny and Gerberich [24] or Oyen and Cook [25]. However, the situation is complicated by the fact that most nanoindenters work in load-controlled mode, and the contact area and pressure in viscoelastic materials under a pointed or spherical indenter change during the test even under constant load. As a consequence, usually only the simplest models are used, able to describe the response only within a relatively narrow time interval or frequency range. Therefore, very often the properties of viscoelastic materials are characterised by single values of hardness and elastic modulus. In these cases, some caution is necessary, as shown below.

In tests with *monotonic loading*, the continuing indenter penetration into the viscoelastic material at the beginning of unloading deforms the unloading curve (Fig. 7). As a consequence, the apparent contact stiffness S_{app}, obtained directly from this curve as $\mathrm{d}P/\mathrm{d}h$, would be incorrect, and thus also the contact depth and area and all quantities calculated from them, such as hardness and, especially, elastic modulus. In order to mitigate the effect of delayed deforming, a dwell under constant load is usually inserted between the loading and unloading periods. According to Chudoba and Richter [26], the distortion of the unloading curve may be neglected if the creep rate during the dwell has decreased so that the indenter penetration does not increase more than 1% per minute. If this condition is not fulfilled, Feng and Ngan [27] recommend to correct the contact stiffness S using the formula:

$$\frac{1}{S} = \frac{1}{S_{\mathrm{app}}} + \frac{\dot{h}_{\mathrm{h}}}{|\dot{P}_{\mathrm{u}}|}, \tag{16}$$

where S_{app} [N/m] is the apparent contact stiffness, $\dot{h}_{\mathrm{h}}$ [m/s] is the indenter velocity at the end of the dwell, and $\dot{P}_{\mathrm{u}}$ [N/s] is the unload rate at the beginning of unloading. While testing viscoelastic–plastic materials, one must not forget that during the dwell (under constant load), the indenter continues penetrating into the specimen, so that the contact area increases and the mean contact pressure at the end of dwell is lower than at its beginning. It is thus impossible to characterise these materials only by a single value of hardness. Test conditions, such as the velocity of loading and

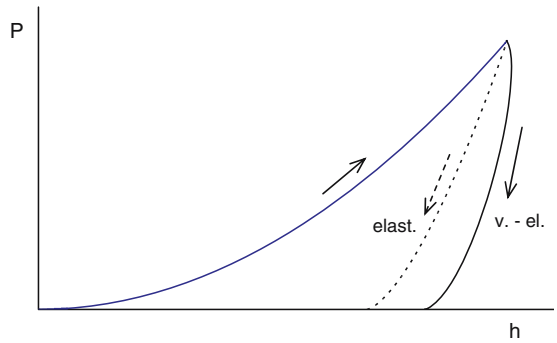

Fig. 7 Load–depth diagram showing unloading curves for an elastic material ("elast.") and a viscoelastic material ("v. - el.")

unloading, and the duration of the dwell, etc., must always be recorded together with the H or E value, so that a comparison with other cases is possible.

The indentation devices working in CSM mode enable the determination of mechanical properties under small *harmonic loading*. For elastic–plastic materials, no significant differences exist between the E and H values obtained in this mode and in the monotonic loading–unloading cycle. With viscoelastic materials, however, the resistance against deforming usually increases with increasing excitation frequency, and so also does the harmonic contact stiffness S_f. Nevertheless, when determining elastic modulus or hardness from indentation tests, it must be kept in mind that the contact area has been created due to the relatively slow monotonic loading, and the minute additional oscillations in the CSM mode had practically no influence on it, cf. Menčík et al. [21]. Thus, the contact depth h_c (and area A) in this mode must be calculated using the contact stiffness S from monotonic unloading! In the determination of harmonic elastic modulus E_f^*, the harmonic contact stiffness S_f corresponding to the frequency f, may be used only in the numerator of Eq. (12). Moreover, though it may seem strange, hardness H calculated according to formula (2) from indenter load P and contact area A, does not depend on the frequency of the small CSM oscillations, but only on the rate of monotonic load increase, the duration of dwell under constant load, and on the velocity of unloading! Thus, all these conditions must always be written together with the particular H value!

Now, a question can be raised: can we somehow characterise the dependence of "hardness" (i.e. the resistance to harmonic indentation loading) on frequency? A simple characteristic is the *index of sensitivity to harmonic loading*, defined by Menčík et al. [21] as the ratio of harmonic and monotonic-unloading contact stiffness for the same contact depth,

$$q_\mathrm{f} = \frac{S_\mathrm{f}}{S}. \tag{17}$$

This characteristic is suitable, for example, for comparing various materials, or for illustrating the influence of exciting frequency f or other test parameters. Because elastic modulus is directly proportional to the contact stiffness, cf. Eqs. (3) and (12), the index q_f also expresses to the ratio of the harmonic and monotonic elastic modulus, $q_\mathrm{f} = E_\mathrm{f}/E$.

More about indentation measurement on various viscoelastic–plastic materials, such as polymers, bones, or bitumen and cement pastes can be found in Ngan and Tang [28], Briscoe et al. [29], Bushby et al. [30] and Pichler et al. [31]. The situation under harmonic loading was analysed in detail by Menčík et al. [21].

11 Creep

Indentation methods can also be used for the determination of viscosity of materials which slowly deform under constant load. Examples are glasses, metals or ceramics at high temperatures (with specially equipped devices), but also some plastics at common temperatures under long-term loading, when the elastic after-effects have died away. The viscosity η is usually calculated from the indenter velocity $\dot{h}$ and load P according to a formula of type

$$\eta = \Psi \ \frac{P}{d_\mathrm{ch}\dot{h}}, \tag{18}$$

where d_ch is the characteristic diameter or other dimension of the indenter, and Ψ is a dimensionless factor, depending on the indenter shape, which is usually a cylinder ("rigid punch"), a cone or a hemisphere. The formula for viscosity can also be written in terms of the total penetration h and duration of loading.

Depth-sensing devices are usually constructed for room temperatures, but some of them can be equipped with special chambers enabling the creep measurement at high temperatures.

More about viscosity measurement can be found, for example, in papers by Brückner and Demharter [32], Cseh et al. [33], or Dorčáková [34] and works quoted therein.

12 Accuracy and errors in depth-sensing indentation

Many factors influence the accuracy of results. First, the indenter can be mentioned. The knowledge of its actual shape is very important especially in nano-indentation tests. If the depth of penetration is several hundreds or even tens of nm, it is not possible to neglect the fact that a pointed indenter has not an ideally sharp tip. Also, the tip of a spherical indenter made of diamond is often not exactly spherical. Moreover, some role is played by the indenter surface quality, which can also gradually deteriorate, especially when very hard materials are tested. Therefore, all indenters must be calibrated. This is usually done by indenting specimens of known properties to various depths, expressing the contact area as a function of contact depth, and finding the constants in this calibration function by fitting it to the measured points. For more details see, e.g. [3]. A role can also be played by the specimen surface finish, and in some cases by the friction or even adhesion between the indenter and specimen.

Another role is played by the elastic modulus of the indenter: the elastic modulus of a specimen is calculated from the (measured) composite modulus (4), consisting of both the specimen and indenter modulus. An error in the indenter modulus thus causes an error in the specimen modulus, especially for materials with very high E. Another problem is the correct setting of the point of initial contact between the indenter and specimen. Further, thermal drift influences not only the apparent (measured) value of contact depth, but, especially, the contact stiffness measured from the unloading curve. This can cause error in contact depth, area and hardness, and, especially, in elastic modulus, more for materials with high elastic modulus. These errors were analysed by Menčík and Swain [35] and recently by Pešek et al. [36]. Another kind of errors is caused by delayed response of viscoelastic materials, e.g. polymers, as was shown earlier in this paper.

A specific problem of instrumented indentation devices without the possibility of direct observation of the imprint is the fact that the shape of the deformed surface around the indenter does not correspond to the theoretical solution for ideal elastic-plastic material. In some cases, the material piles up around the indenter, so that the actual contact area is larger and the apparent measured contact depth is smaller than it would be without the uplift. As a consequence, the apparent values of elastic modulus and hardness are higher than the actual values. Piling up can be expected for ductile soft materials, and also for soft coatings on a hard stiff substrate, where the radial flow of the film material away from the indenter is restrained by the substrate. In the opposite case, for relatively hard materials, so-called sink-in sometimes appears: due to larger depression of the material outside the indent, the apparent contact depth and area is smaller, and the measured modulus and hardness are lower than the actual values. There are several papers on this topic. For the information about pile-up, which appears more often, the reader is referred to Oliver and Pharr [4] and the works quoted therein.

The accuracy of results also depends on the type of device used. For example, some devices eliminate the influence of thermal drift, while some not. It is impossible to analyse here the individual types. The only universal advice when choosing a device for certain task is to be aware of possible errors, as discussed in this paragraph and in the quoted papers.

13 Other information from instrumented indentation, conclusion

In addition to the properties discussed in this paper, depth-sensing indentation can yield extra information, for example by analysing the shape of loading and unloading curves. Discontinuities or sudden changes in the slope indicate formation of cracks in a brittle material or delamination of a coating, plastic flow, or even high-pressure-induced phase transformations, arising, e.g., in silicon (Si) during indenter unloading. Further information can be obtained

if the indentation device is combined with atomic force microscope enabling observation of the imprints and more accurate characterisation of their shape, or with equipment for acoustic emission, which can indicate irreversible phenomena in the material. Some devices enable also the specimen movement in the tangential direction, and measure both the normal and tangential component of indenter load and movement, and analyse the friction. This topic, however, goes beyond the scope of this paper.

There are various devices for instrumented indentation, especially for very low loads (often called "nanoindenters"), but also devices working with loads up to tens of N. More information on individual products can be found at manufacturers of advanced hardness testers and other devices for testing of mechanical properties.

During the last 20 years, devices for depth-sensing indentation have made a big progress, and their development is not at the end yet. The instrumented indentation has significantly extended the amount of our information on the mechanical behaviour of many materials, from metals and ceramics, over plastics and biologic tissues, to thin films and other special products, often of new composition, microstructure and properties. The "intelligent indenters" have become an indispensable tool for materials research, as well as for development and production.

Acknowledgements This work was supported by the Grant Agency of the Czech Republic, Projects No.103/05/2066 and No. 101/04/0033.

References

1. ISO 14577. Metallic materials – Instrumented indentation test for hardness and materials parameters. Part 1 – Test method, Part 2: Verification and calibration of testing machines, Part 3: Calibration of reference blocks, Part 4: Test method for metallic and non-metallic coatings, 2002–2004
2. Fischer-Cripps AC (2002) Nanoindentation. Springer, New York
3. Oliver WC, Pharr GM (1992) An improved technique for determining hardness and elastic modulus using load and displacement sensing indentation experiments. J Mater Res 7:1564–1583
4. Oliver WC, Pharr GM (2004) Measurement of hardness and elastic modulus by instrumented indentation: advances in understanding and refinements to methodology. J Mater Res 19:3–20
5. Sneddon IN (1965) The relation between load and penetration in the axisymmetric Boussinesq problem for a punch of arbitrary profile. Int J Engng Sci 3:47–51
6. Tabor H (1951) Hardness of metals. Clarendon Press, Oxford
7. Herbert EG, Pharr GM, Oliver WC, Lucas BN, Hay JL (2001) On the measurement of stress-strain curves by spherical indentation. Thin Solid Films 398–399: 331–335
8. Johnson KL (1985) Contact mechanics. Cambridge University Press, Cambridge
9. Mesarovic SDj, Fleck NA (1999) Spherical indentation into elastic-plastic solids. Proc R Soc Lond A 455:2707–2728
10. Menčík J (2006) Determination of stress-strain curves by instrumented indentation. 23rd Danubia Adria symposium on experimental methods in solid mechanics, Podbanské, 26–29 Sept 2006, University of Žilina
11. Field J, Swain MV (1993) A simple predictive model for spherical indentation. J Mater Res 8:297–306
12. Kružík M, Mielke A, Roubíček T (2005) Modelling of microstructure and its evolution in shape-memory-alloy single-crystals, in particular in CuAlNi. Meccanica 40:389–418
13. Sakai M (1993) Energy principle of the indentation-induced inelastic surface deformation and hardness of brittle materials. Acta Metall Mater 40:1751–1758
14. Menčík J, Swain MV (1994) Characterisation of materials using micro-indentation tests with pointed indenters. Mater Forum 18:277–288
15. Menčík J, Munz D, Quandt E, Weppelmann ER, Swain MV (1997) Determination of elastic modulus of thin layers using nanoindentation. J Mater Res 12:2475–2484
16. Gao H, Chiu CH, Lee J (1992) Elastic contact versus indentation modelling of multilayered materials. Int J Solids Struct 29:2471–2492
17. Burnett PJ, Rickerby DS (1987) The mechanical properties of wear resistant coatings I, II: modelling of hardness behaviour. Thin Solid Films 148:41–65
18. Jönsson B, Hogmark S (1984) Hardness measurement of thin films. Thin Solid Films 114:257–269
19. Bhattacharya AK, Nix WD (1988) Analysis of elastic and plastic deformation associated with indentation testing of thin films on substrates. Int J Solids Struct 24:1287–1298
20. Menčík J (1996) Mechanics of components with treated or coated surfaces. Kluwer Academic Publishers, Dordrecht
21. Menčík J, Rauchs G, Bardon J, Riche A (2005) Determination of elastic modulus and hardness of viscoelastic-plastic materials by instrumented indentation under harmonic load. J Mater Res 20:2660–2669
22. Haddad YM (1995) Viscoelasticity of engineering materials. Chapman & Hall, London
23. Tschoegl NW (1989) The phenomenological theory of linear viscoelastic behavior. Springer-Verlag, Berlin
24. Strojny A, Gerberich WW (1988) Experimental analysis of viscoelastic behavior in nanoindentation.

In: Moody NR, Gerberich WW, Burnham N, Baker SP (eds) Fundamentals of nanoindentation and nanotribology. Mat. Res. Soc. Symp. Proc. 522, MRS, Warrendale, Pennsylvania, pp 159–164
25. Oyen ML, Cook RF (2003) Load displacement behavior during sharp indentation of viscous-elastic-plastic materials. J Mater Res 18:139–150
26. Chudoba T, Richter F (2001) Investigation of creep behaviour under load during indentation experiments and its influence on hardness and modulus results. Surf Coat Technol 148:191–198
27. Feng G, Ngan AHW (2002) Effects of creep and thermal drift on modulus measurement using depth-sensing indentation. J Mater Res 17:660–668
28. Ngan AHW, Tang B (2002) Viscoelastic effects during unloading in depth-sensing indentation. J Mater Res 17:2604–2610
29. Briscoe BJ, Fiori L, Pelillo E (1998) Nano-indentation of polymeric surfaces. J Phys D Appl Phys 31: 2395–2405
30. Bushby AJ, Ferguson VL, Boyde A (2003) Nanoindentation of bone: Comparison of specimen tested in liquid and embedded in polymethylmethacrylate. J Mater Res 19:249–259
31. Pichler Ch, Jäger A, Lackner R, Eberhardsteiner J (2005) Identification of material properties from nanoindentation: application to bitumen and cement paste. 22nd Danubia Adria symposium on experimental methods in solid mechanics, Monticelli, 28 Sept – 1 Oct 2005, University of Parma, pp 198–199
32. Brückner R, Demharter G (1975) Systematische Untersuchungen über die Anwendbarkeit von Penetrationsviskosimetern. Glastech Ber 48:12–18
33. Cseh G, Chinh NQ, Tasnádi A, Juhász A (1997) Indentation test for the investigation of high-temperature plasticity of materials. J Mater Sci 32:5107–5111
34. Dorčáková F, Jan V, Špaková J, Dusza J (2005) Indentation creep in advanced ceramics research. 2nd Slovak-Czech conference "local mechanical properties", 14–15 November, Košice, Slovak Republic. Technical University of Košice, CD-ROM, ISBN 80-8073-405-4
35. Menčík J, Swain MV (1995) Errors asociated with depth-sensing microindentation tests. J Mater Res 10:1491–1501
36. Pešek L, Zubko P, Vadasová Z, Ambriško L (2005) Mechanical properties of reference blocks for instrumented hardness measurement and factors affecting measurement accuracy. 2nd Slovak-Czech conference "local mechanical properties", 14–15 November 2005, Košice, Slovak Republic. Technical University of Košice, CD-ROM, ISBN 80-8073-405-4